nature biotechnology

Sequential treatment of drug-resistant tumors with targeted minicells containing siRNA or a cytotoxic drug

Jennifer A MacDiarmid[1], Nancy B Amaro-Mugridge[1], Jocelyn Madrid-Weiss[1], Ilya Sedliarou[1], Stefanie Wetzel[1], Kartini Kochar[1], Vatsala N Brahmbhatt[1], Leo Phillips[1], Scott T Pattison[1], Carlotta Petti[1], Bruce Stillman[2], Robert M Graham[3,4] & Himanshu Brahmbhatt[1]

The dose-limiting toxicity of chemotherapeutics, heterogeneity and drug resistance of cancer cells, and difficulties of targeted delivery to tumors all pose daunting challenges to effective cancer therapy. We report that small interfering RNA (siRNA) duplexes readily penetrate intact bacterially derived minicells previously shown to cause tumor stabilization and regression when packaged with chemotherapeutics. When targeted via antibodies to tumor-cell-surface receptors, minicells can specifically and sequentially deliver to tumor xenografts first siRNAs or short hairpin RNA (shRNA)–encoding plasmids to compromise drug resistance by knocking down a multidrug resistance protein. Subsequent administration of targeted minicells containing cytotoxic drugs eliminate formerly drug-resistant tumors. The two waves of treatment, involving minicells loaded with both types of payload, enable complete survival without toxicity in mice with tumor xenografts, while involving several thousandfold less drug, siRNA and antibody than needed for conventional systemic administration of cancer therapies.

RNA interference (RNAi) is a natural phenomenon resulting in potent post-transcriptional gene silencing produced by double-stranded RNAs that occur in most eukaryotes[1]. This multistep process, which is initiated by double-stranded 21- to 23-nucleotide noncoding siRNAs or microRNAs, results in highly efficient and sequence-specific knockdown of the targeted gene's expression. siRNAs can also be expressed from plasmid DNAs as shRNAs using an RNA polymerase III promoter.

Despite the considerable potential of RNAi for treating cancer[2], several challenges need to be overcome for exogenous siRNA to be widely used as a cancer therapeutic. These include: (i) lability of siRNAs, resulting in rapid degradation by serum nucleases, (ii) poor membrane permeability to siRNAs, limiting cellular uptake, (iii) the need for effective design of active siRNAs to ensure optimal gene silencing activity with minimal 'off-target' effects and (iv) the need to achieve efficient intracellular delivery to target cells *in vivo*[3]. Several promising strategies have been developed for systemic siRNA delivery. These include nanoparticles[4], aptamer-siRNA conjugates[5], nanoimmunoliposomes[6], cationic polymer and lipid-based siRNA complexes[7]. Nonetheless, several hurdles remain.

We previously reported that minicells, produced by derepressing cryptic polar sites of cell fission through inactivating genes controlling normal bacterial cell division[8], can be packaged with therapeutically relevant concentrations of a range of chemotherapeutics. These minicells, selectively targeted to cancer cells via bispecific antibodies (BsAb), effect substantial tumor stabilization or regression in a variety of tumor xenograft models, as well as in dogs with endogenous tumors[9,10]. Recently, siRNA has been used to downregulate proteins involved in cancer survival and proliferation such as ribonucleotide reductase[11] and Protease-Activated Receptor-1[12]. We now report that, somewhat unexpectedly, siRNAs readily traverse the intact outer and inner membranes of minicells. Moreover, minicells targeted to tumors via BsAb, packaged with siRNAs or plasmid encoding shRNAs, can effectively suppress expression of critical cell cycle–associated proteins implicated in tumor cell proliferation. Minicell-delivered siRNAs or shRNAs specific for polo-like kinase 1 (PLK1)[13], kinesin spindle protein (KSP (KIF11))[14] and cyclin-dependent kinase 1 (CDK1)[15] effect potent G2 arrest and apoptosis of tumor cells both *in vitro* and *in vivo*.

We next conducted proof-of-concept studies involving minicell-delivered therapies to treat drug-resistant cancers. Chemosensitization of multi-drug resistant tumor cells following adenoviral delivery of anti-*MDR1* (also known as *ABCB1*) shRNAs *in vitro* has been reported[16], but viral vectors do not have the dual capacity of shRNA and drug delivery and successful targeting of tumor cells *in vivo* remains problematic. Our strategy involved dual sequential treatments that first target a known drug resistance mechanism (e.g., overexpression of the multi-drug resistance P-glycoprotein MDR1[17]) by means of si/shRNA-containing minicells targeted to tumors via BsAb. After allowing for sufficient time to achieve substantial knockdown of the drug-resistance mediating protein, we followed this with a second wave of therapy involving intravenous (i.v.) administration of BsAb-targeted minicells packaged with cytotoxic drug. Our approach rendered drug-resistant tumor xenografts

[1]EnGeneIC Pty Ltd., Sydney, New South Wales, Australia. [2]Cold Spring Harbor Laboratory, Cold Spring Harbor, New York, USA. [3]Victor Chang Cardiac Research Institute, Darlinghurst, New South Wales, Australia. [4]University of New South Wales, Kensington, New South Wales, Australia. Correspondence should be addressed to H.B. (hbrahmbhatt@engeneic.com).

Received 3 May; accepted 1 June; published online 28 June 2009; doi:10.1038/nbt.1547

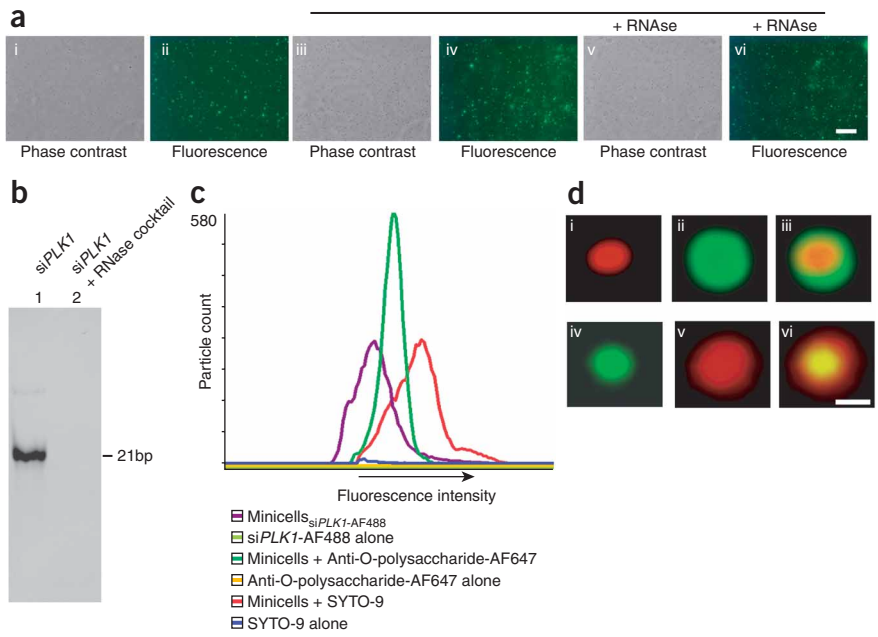

Figure 1 siRNA packaging in minicells, loading efficiency and BsAb targeting of the siRNA-packaged minicells to tumor cells. (**a**) Minicells were loaded with fluorescent AF488-tagged si*PLK1* (i,ii) or with AF488-tagged si*KSP* (iii–vi) and examined by phase contrast and fluorescence microscopy. Comparison of the phase contrast and fluorescence images reveals that most of the minicells are loaded with fluorescently labeled siRNA, and that the fluorescence of minicells$_{si\mathit{KSP}\text{-AF488}}$ (iv) remains largely unchanged after RNase treatment (vi), as also shown quantitatively (**c**). Scale bar, 25 μm. (**b**) si*PLK1* was co-incubated with RNase cocktail for 30 min at 37 °C and resolved by 20% SDS-PAGE. This shows complete degradation of si*PLK1* by the RNase cocktail used in **a** (v,vi). (**c**) FACS analysis for minicell quantification and determination of siRNA packaging efficiency in minicells. Minicells were quantified by labeling with the cell-permeant fluorescent dye SYTO-9, packaged in minicells as described previously[9]. Minicells (50,000) were stained with SYTO-9 or by minicell-surface O-polysaccharide labeling, using an AF647-tagged monoclonal antibody against O-polysaccharide. An additional 50,000 minicells were incubated with si*PLK1*-AF488 and processed as described. The SYTO-9- and anti-O-poly/AF647-labeled minicells were also processed in the same way but in the absence of si*PLK1*-AF488 to keep minicell losses during processing constant for all samples. The area under both the minicells + SYTO-9 and minicells + anti-O-poly/AF647 curves are identical (44,000 ± 1,000 minicells; loss in processing being ~6,000), indicating that both labeling methods enumerated the same number of minicells. The area under the minicell$_{si\mathit{PLK1}\text{-AF488}}$ curve is ~80% (36,000 ± 1,000 minicells) of that of either of the above fluorescence curves, indicating that ~80% of the minicells are packaged with AF488-tagged si*PLK1*. (**d**) BsAb-targeted, siRNA-containing minicells visualized by fluorescence microscopy. (i) AF555-tagged si*MDR1* (red fluorescence) packaged in minicells; (ii) surface O-polysaccharide labeling of minicell by AF488-tagged (green fluorescence) BsAbs; (iii) overlay of images (i) and (ii); (iv) AF488-tagged si*KSP* (green fluorescence) packaged in minicells; (v) surface O-polysaccharide labeling of minicell by AF647 (red fluorescence)-tagged BsAbs, and (vi) overlay of images (iv) and (v). Scale bar, 5 μm.

sensitive to cytotoxic drugs and enabled complete survival even of mice bearing aggressive human tumor xenografts.

RESULTS

Packaging siRNA into minicells and targeting tumor cells

Minicells were derived from a *min*CDE$^-$ chromosomal deletion mutant of *Salmonella enterica* serovar Typhimurium (*S. typhimurium*) and purified as described previously[9]. Alexa Fluor (AF)488-tagged siRNAs targeting *PLK1* or *KSP* (designated minicells$_{si\mathit{PLK1}\text{-AF488}}$ and minicells$_{si\mathit{KSP}\text{-AF488}}$, respectively) were incubated with minicells overnight with gentle agitation and were visualized by fluorescence microscopy. Most minicells fluoresced bright green (**Fig. 1**), indicating that AF488-tagged siRNAs are concentrated within the minicell cytosol and periplasmic space. The intense green fluorescence remained unchanged after incubation with an RNase cocktail (**Fig. 1a**, v,vi), which in preliminary studies was shown to cause complete siRNA degradation (**Fig. 1b**). This suggests that the siRNA was not adhering nonspecifically to the minicell surface. Similarly, vigorous and repeated washing of the siRNA-containing minicells did not decrease fluorescence.

We used fluorescence-activated cell sorting (FACS) to demonstrate efficient siRNA packaging in minicells. Minicells$_{si\mathit{PLK1}\text{-AF488}}$ were quantified relative to the total number of minicells in the incubation solution. The latter were quantified by staining of endogenous minicell RNA using SYTO-9, as described previously[9]. As the intrinsic fluorescence of chemotherapeutic drugs packaged into minicells can interfere with SYTO-9 fluorescence, we developed an independent method of minicell quantification involving labeling minicells with an AF647-tagged anti-O-polysaccharide monoclonal antibody, designated anti-O-poly/AF647. The rationale was to use a fluorescent dye linked to the exterior of the minicell to avoid fluorescence interference from drugs packaged within the minicell cytoplasm. The SYTO-9 and anti-O-poly/AF647 methods gave similar results (**Fig. 1c**), indicating that 44,000 ± 1,000 of 50,000 ± 1,000 minicells were packaged in both cases. After siRNA loading, >80% of minicells were routinely packaged with siRNA (36,000 ± 1,000 minicells of the 44,000 ± 1,000 minicells enumerated by the two methods above). The observation that treatment with RNase did not affect the fluorescence intensity and the number of minicells enumerated by FACS (data not shown) further suggests that it is unlikely that the siRNAs adhered nonspecifically to the minicell surface.

We used quantitative PCR of siRNA extracted from minicells$_{si\mathit{KSP}}$ to estimate 300 ± 30 ng of siRNA/10^9 minicells, or ~12,000 molecules of siRNA/minicell (data not shown).

To package shRNA into minicells, we transformed the parent *S. typhimurium min*CDE$^-$ mutant strain with plasmid DNA encoding shRNA. As demonstrated previously[18], this results in plasmid segregation into daughter minicells. Plasmid extraction and purification from recombinant minicells routinely yielded ~4 ± 1 μg plasmid DNA in 10^{10} minicells, equating to ~100 plasmid copies per minicell.

We used BsAb to target recombinant minicells to tumor cells, as described previously[9]. One arm of these antibodies recognizes the O-polysaccharide component of the minicell surface lipopolysaccharide and the other, a tumor-preferential cell surface–receptor, such as the epidermal growth factor receptor (EGFR), which is overexpressed in several cancers[19].

Figure 1d shows a BsAb-targeted, siRNA-containing minicell visualized by fluorescence microscopy. The red fluorescence of

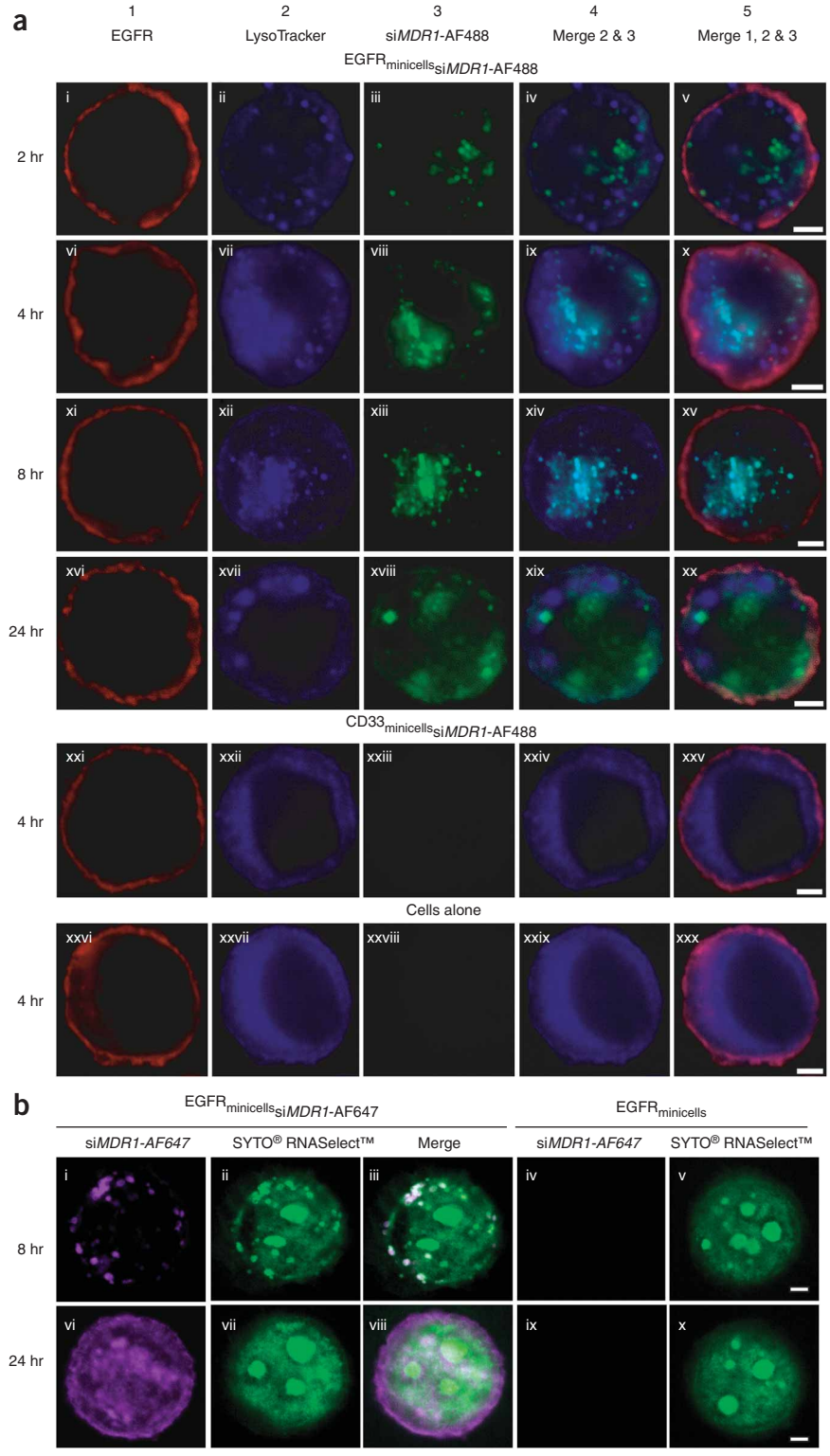

Figure 2 Intracellular fate of siRNA-containing minicells targeted to human cancer cells and cytoplasmic release of siRNA. (**a**) Human uterine cancer cells, MES-SA/Dx5, were treated with specifically or nonspecifically targeted ^{EGFR}minicells$_{si\mathit{MDR1}\text{-AF488}}$ or ^{CD33}minicells$_{si\mathit{MDR1}\text{-AF488}}$, respectively. Nontransfected cells were included as controls. The cells were visualized by confocal microscopy over 24 h. MES-SA/Dx5 cell membranes were visualized using AF594-conjugated anti-EGFR mAb (red fluorescence); minicells carrying si*MDR1*-AF488 were revealed by AF488-mediated green fluorescence, and intracellular acidified lysosomes were visualized using LysoTracker Blue DND-22 dye (navy blue fluorescence). The images shown are for MES-SA/Dx5 cells treated with ^{EGFR}minicells$_{si\mathit{MDR1}\text{-AF488}}$ (2 h, i–v; 4 h, vi–x; 8 h, xi–xv; 24 h, xvi–xx), ^{CD33}minicells$_{si\mathit{MDR1}\text{-AF488}}$ (4 h, xxi–xxv) and cells alone (4 h, xxvi–xxx). Overlaid images are shown in lanes 4 (images from lanes 2 and 3) and 5 (images from lanes 1, 2 and 3). Co-localization of LysoTracker dye (navy blue fluorescence) and ^{EGFR}minicells$_{si\mathit{MDR1}\text{-AF488}}$ (green fluorescence) results in light blue fluorescence observed in images ix and xiv. Scale bar, 5 μm. (**b**) MES-SA/Dx5 cells were treated with ^{EGFR}minicells$_{si\mathit{MDR1}\text{-AF647}}$ or ^{EGFR}minicells (control). Nontransfected cells were included as controls and cells were visualized by confocal microscopy over 24 h. si*MDR1*-AF647 was revealed by the AF647-mediated violet fluorescence and RNAs were detected using the RNA-selective SYTO RNASelect dye (green fluorescence). The images shown are for MES-SA/Dx5 cells treated with ^{EGFR}minicells$_{si\mathit{MDR1}\text{-AF647}}$ (8 h, i–iii; 24 h, vi–viii), and ^{EGFR}minicells (8 h, iv,v; 24 h, ix,x). Co-localization of si*MDR1*-AF647 and SYTO RNASelect dye results in white fluorescence (iii,viii). No violet AF647 fluorescence was observed in cells treated with ^{EGFR}minicells not carrying si*MDR1*-AF647 (iv,ix). Scale bar, 5 μm.

AF555-tagged si*MDR1* packaged within minicells (**Fig. 1d**, i) and the green fluorescence of AF488-tagged BsAb coating the outer surface of the minicells (**Fig. 1d**, ii) are evident. The coincident central orange fluorescence when these images are overlaid (**Fig. 1d**, iii) indicates co-localization of the BsAb covering the minicell surface and siRNA within the minicells. A similar observation was also evident for the overlay (yellow fluorescence; **Fig. 1d**, vi) of AF488-tagged si*KSP* (green fluorescence; **Fig. 1d**, iv) packaged in minicells with AF647-tagged BsAb (red fluorescence; **Fig. 1d**, v) bound to the outer surface of the minicell.

An ~80% transfection efficiency of tumor cells was demonstrated using minicell-mediated siRNA delivery, as detailed in **Supplementary Results** and **Figure 1**.

Intracellular kinetics of siRNA delivery via targeted minicells

We demonstrated previously[9] that drug-containing minicells targeted via BsAb specifically bound to tumor cell-surface receptors were internalized by receptor-mediated endocytosis and degraded in intracellular vacuoles. The minicell cargo was released from degraded minicells and entered the cytoplasm and nucleus of the tumor cell, resulting in cell death.

To determine the intracellular fate of human cancer cells targeted by siRNA-containing minicells, we incubated human uterine cancer cells with EGFR-targeted, si*MDR1*-AF488 packaged minicells, designated as

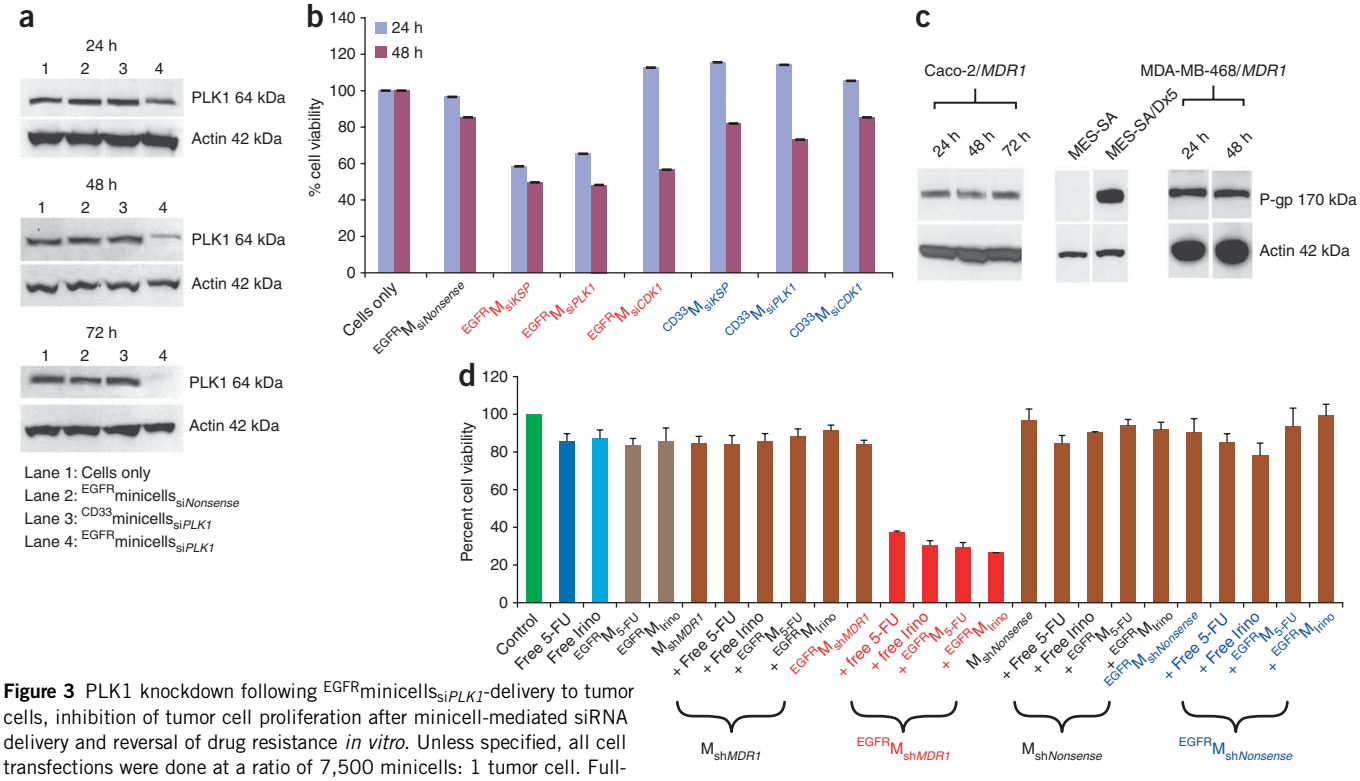

Figure 3 PLK1 knockdown following ^{EGFR}minicells$_{siPLK1}$-delivery to tumor cells, inhibition of tumor cell proliferation after minicell-mediated siRNA delivery and reversal of drug resistance *in vitro*. Unless specified, all cell transfections were done at a ratio of 7,500 minicells: 1 tumor cell. Full-length blots are provided in **Supplementary Figure 5**. Error bars indicate ± s.e.m. (**a**) HCT116 cells were treated with ^{EGFR}minicells$_{siPLK1}$, and cells were processed for immunoblotting at 24, 48 and 72 h post-transfection. Anti-PLK1 and anti-actin (loading control) monoclonal antibodies were used as primary antibodies to reveal the respective proteins. Cells transfected with control ^{EGFR}minicells$_{siNonsense}$ or ^{CD33}minicells$_{siPLK1}$ showed unchanged PLK1 levels relative to the untreated control cells, whereas ^{EGFR}minicells$_{siPLK1}$-treated cells showed substantial knockdown of PLK1 by 48 and 72 h. (**b**) HCT116 cells were incubated (in triplicate) with ^{EGFR}minicells$_{siPLK1}$, ^{EGFR}minicells$_{siKSP}$ or ^{EGFR}minicells$_{siCDK1}$. Excess minicells were washed off after 2 h co-incubation and cell viability was determined using the MTT assay 24 and 48 h thereafter. ^{EGFR}minicells$_{siPLK1}$ and ^{EGFR}minicells$_{siKSP}$ treatments inhibited cell viability at both times ($P < 0.0001$ in each case versus cells alone) and ^{EGFR}minicells$_{siCDK1}$ inhibited cell proliferation by 48 h. Control cells were either untreated or treated with ^{EGFR}minicells$_{siNonsense}$, or minicells targeted to an irrelevant antigen (^{CD33}M$_{siKSP, -PLK1}$ or $_{-CDK1}$). By 48 h, small nonsignificant changes in proliferation were observed after treatment with ^{CD33}minicells or ^{EGFR}minicells$_{siNonsense}$ relative to untreated cells. These likely result from the technical hurdle of completely washing away minicells nonspecifically bound to tumor cells in tissue culture. (**c**) Immunoblotting of cell extracts from Caco-2/MDR1, MDA-MB-468/MDR1 and MES-SA/Dx5 multidrug-resistant cell lines with anti-P-gp and anti-actin (loading control) monoclonal antibodies as the primary antibodies, showing constitutive expression of P-gp. The control drug-sensitive cell line MES-SA does not express P-gp. Cells were processed for western blotting after culture for 24, 48 and 72 h (Caco-2/MDR1), 24 h (MES-SA and MES-SA/Dx5), or 24 and 48 h (MDA-MB-468/MDR1). (**d**) Caco-2/MDR1 cells were transfected (in triplicate) with ^{EGFR}minicells$_{shMDR1}$ as described in **c** and followed 24 h later by treatment with ^{EGFR}minicells$_{irinotecan}$ or ^{EGFR}minicells$_{5\text{-}FU}$ (both at 5,000 minicells/cell; 80 ng and 40 ng irinotecan and 5-FU carried in 1×10^9 minicells per well respectively) or free drugs (irinotecan or 5-FU; 25 μM/well of each). The various control treatments are shown in the figure. Cell viability was determined using the MTT assay, 72 h later. Highly significant inhibition of cell viability was evident following dual treatment of ^{EGFR}minicells$_{shMDR1}$ followed by ^{EGFR}minicells$_{irinotecan}$ or ^{EGFR}minicells$_{5\text{-}FU}$ or free drugs ($P < 0.0001$ in each case versus cells alone), indicating reversal of drug resistance. Irino, irinotecan.

^{EGFR}minicells$_{siMDR1\text{-}AF488}$ (green fluorescence), and monitored their fate over 24 h using confocal microscopy. Intracellular acidic organelles, lysosomes, were stained with LysoTracker (navy blue fluorescence) and EGFR bound to the tumor cell surface was revealed using anti-EGFR-AF594 MAb (red fluorescence). We used ^{CD33}minicells$_{siMDR1\text{-}AF488}$, where the BsAb is directed against CD33 (an antigen not found on the surface of MES-SA/Dx5 cells; data not shown), as a control. ^{CD33}minicells$_{siMDR1\text{-}AF488}$ did not adhere to the MES-SA/Dx5 cell surface (**Fig. 2a**, xxiii) and were not internalized (as indicted by the absence of green fluorescence). However, by 2 h after transfection, ^{EGFR}minicells$_{siMDR1\text{-}AF488}$ treated cells showed large numbers of intracellular minicells (green fluorescence; **Fig. 2a**, iii). This corroborates our previous results[9] and shows that minicells specifically target to tumor cells via BsAbs directed against overexpressed cell surface antigens, entering the cytoplasm by receptor-mediated endocytosis. Once internalized, minicells track to lysosomes, as evidenced by the light blue fluorescence (see **Fig. 2a**, ix, xiv, for example) resulting from coincident LysoTracker (navy blue) and AF488 (green) labeling seen in the overlaid ^{EGFR}minicells$_{siMDR1\text{-}AF488}$ and LysoTracker images. LysoTracker staining was more intense after 4 h or 8 h (**Fig. 2a**, vii, xii) than after 2 h (**Fig. 2a**, ii). This suggests both internalization of a substantial number of minicells (**Fig. 2a**, viii, xiii) and that the intracellular activity of endosome/lysosome fusion had intensified as a result of late lysosome acidification, which enabled minicell degradation.

By 24 h, si*MDR1*-AF488 was released from degraded minicells and surprisingly, escaped in significant quantities from the lysosomal membrane and entered the cytoplasm, as was evident from the diffuse green fluorescence throughout the cytoplasm (**Fig. 2a**, xviii. xix). To determine whether this fluorescence was associated with si*MDR1*-AF488 or simply fluorophore cleaved from the siRNA, we carried out additional experiments involving ^{EGFR}minicells that carry si*MDR1*-AF647 (violet fluorescence). Tracking the minicells for 24 h post-transfection using the RNA-selective dye SYTO RNASelect (green fluorescence) showed that by 8 h, the violet fluorescence was

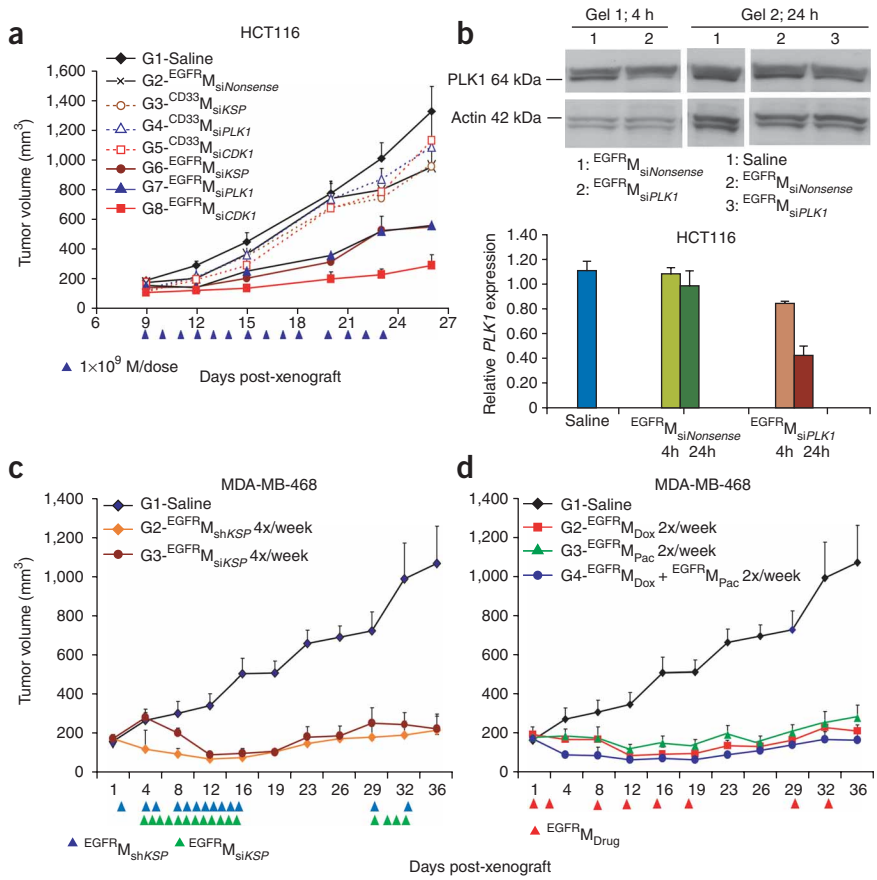

Figure 4 Inhibition of xenograft tumor–growth following minicell-mediated delivery of si/sh RNAs against cell cycle–associated proteins and target mRNA/protein knockdown *in vivo*. All minicell doses were administered intravenously in nude mice with 10^9 minicells per dose. The concentrations of siRNAs or shRNA or drug administered per dose in 10^9 minicells include, (**a**) ~300 ng siRNA, (**b**) ~10^{11} copies of shRNA, (**c**) ~0.8 μg doxorubicin, (**d**) ~0.03 μg paclitaxel. The days when the various minicell treatments were administered are shown below the *x*-axis. Error bars indicate ± s.e.m. Full-length blots are provided in **Supplementary Figure 5**. (**a**) HCT116 xenografts ($n = 8$/group) were treated on the days indicated below the *x*-axis, with ^{EGFR}minicells$_{siKSP, -PLK1}$ or $_{-CDK1}$ (designated $^{EGFR}M_{siKSP}$, $^{EGFR}M_{siPLK1}$ and $^{EGFR}M_{siCDK1}$, respectively). All treatments produced potent antitumor effects ($P < 0.0001$ in each case at 26 d), compared with untreated controls (saline), or controls treated with ^{EGFR}minicells$_{siNonsense}$ (designated $^{EGFR}M_{siNonsense}$) or ^{CD33}minicells$_{siKSP, -PLK1}$ or $_{-CDK1}$ (designated $^{CD33}M_{siKSP, -PLK1}$ or $_{-CDK1}$). No antitumor effects were observed with the various controls used. (**b**) Western blots were from total protein derived from resected tumors (4 and 24 h) from a repeat xenograft in **a**, with three mice per group. The mice received four i.v. doses of ^{EGFR}minicells$_{siPLK1}$ or ^{EGFR}minicells$_{siNonsense}$ or saline control, 24 h apart. Total protein immunoblots were developed with either anti-PLK1 or anti-actin (control) monoclonal antibodies. Total RNA was also extracted from a third of the tumor mass from each mouse and after conversion to cDNA, was processed for real-time PCR using *PLK1*- and *GAPDH* (control)-specific primers. The PCR data are shown below the western blot. By 4 h and 24 h after the last dose of ^{EGFR}minicells$_{siPLK1}$, substantial knockdown of PLK1 target protein (bottom of the two bands) was observed. Similarly, *PLK1* mRNA knockdown at the same time points was highly significant (4 h and 24 h; $P < 0.0014$ and $P < 0.0029$, respectively). (**c**) MDA-MB-468 human breast cancer xenografts ($n = 8$/group) were untreated (saline controls) or treated with the EGFR-targeted minicells indicated (see **a** for minicell designations). Inhibition of tumor growth is evident as early as day 8 in all treatment groups and tumor volumes remained stable until the experiment was terminated at day 36 ($P < 0.0001$ for tumor volume in each treatment group versus saline control). (**d**) Same xenograft as in **c** but treatments included EGFR-targeted minicells packaged with doxorubicin or paclitaxel. Inhibition of tumor growth is similar to that seen in **c**.

concentrated in a few parts of the cell (**Fig. 2b**, i), presumably within endosomes or lysosomes (**Fig. 2a**, ix, xiv), as previously demonstrated[9]. By 24 h, diffuse violet fluorescence was evident throughout the cytoplasm (**Fig. 2b**, vi). By 8 h, the concentrated violet fluorescence (**Fig. 2b**, i) appeared as white fluorescence (overlaid green and violet; **Fig. 2b**, iii), and by 24 h diffuse white fluorescence replaced the violet fluorescence (**Fig. 2b**, viii). This corroborates observations (**Fig. 2a**, xviii) that si*MDR1*-AF647 was not cleaved to release the fluorophore but, that instead, si*MDR1*-AF647 was likely released intact into the cytoplasm after 24 h.

siRNA delivery to cancer cells *in vitro*

To assess whether minicell-mediated delivery of siRNA against cell cycle proteins, such as PLK1, would result in target-protein knockdown, we treated human colorectal carcinoma (HCT116) cells with ^{EGFR}minicells$_{siPLK1}$. The steady state expression of PLK1 protein was substantially inhibited by 48 h (**Fig. 3a**) and was barely detectable by 72 h. These findings are consistent with observations that ^{EGFR}minicells$_{siPLK1}$ induce cell cycle arrest (**Supplementary Fig. 1**) with resulting inhibition of tumor-cell proliferation (described below in **Fig. 3b**).

We also showed that minicells targeted via BsAb and containing siRNAs directed against critical cell cycle–associated proteins could inhibit tumor-cell proliferation. When HCT116 cells were transfected with ^{EGFR}minicells$_{siPLK1}$, ^{EGFR}minicells$_{siKSP}$ or ^{EGFR}minicells$_{siCDK1}$ (**Fig. 3b**), cell proliferation was inhibited by ~52%, 51% and 44%, respectively after 48 h.

Minicell-mediated siRNA delivery reverses drug resistance *in vitro*

We next sought to determine whether drug-resistant tumor cells could be killed by initially overcoming drug resistance by minicell-mediated delivery of si/shRNA targeting *MDR1*, and then treating the same cells with targeted, cytotoxic drug–packaged minicells.

For these studies, we established a variant (Caco-2/MDR1) of Caco-2 colon cancer cells that constitutively overexpresses MDR1 (**Fig. 3c**) and is resistant to both 5-fluorouracil (5-FU) and irinotecan (Camptosar) (data not shown).

Caco-2/MDR1 cells were treated with ^{EGFR}minicells$_{shMDR1}$ followed 24 h later by ^{EGFR}minicells$_{irinotecan}$ or ^{EGFR}minicells$_{5\text{-}FU}$. Only the dual treatment protocol involving initial exposure of Caco-2/MDR1 cells to ^{EGFR}minicells$_{shMDR1}$ followed by treatment with irinotecan, 5-FU, ^{EGFR}minicells$_{irinotecan}$ or ^{EGFR}minicells$_{5\text{-}FU}$, showed highly significant ($P < 0.0001$, relative to untreated cells) cytotoxicity with 69%, 62%, 74% and 70% inhibition of cell growth (**Fig. 3d**), respectively.

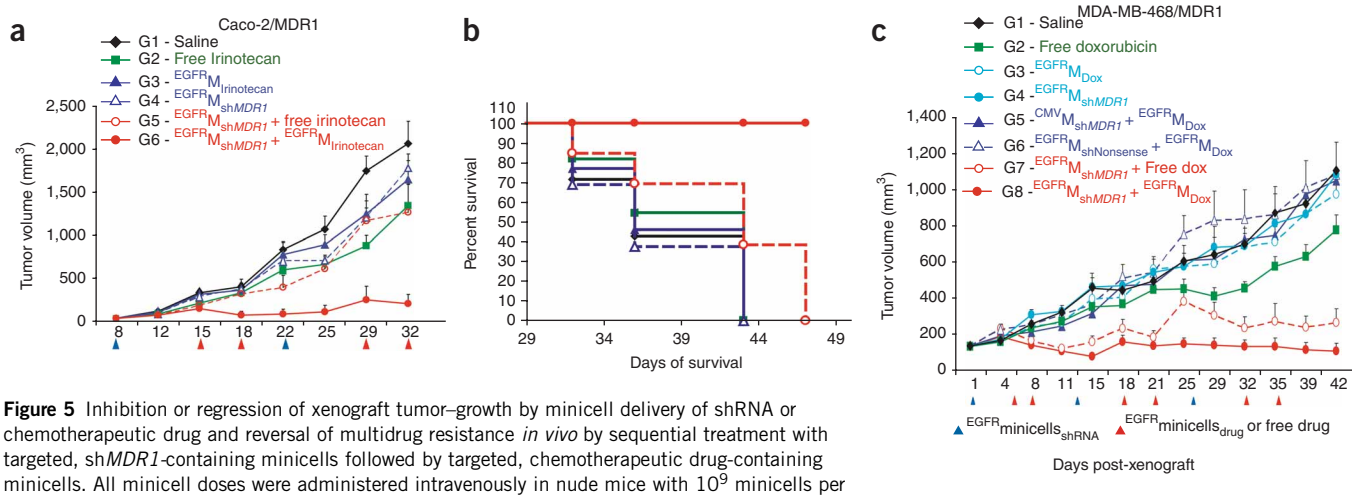

Figure 5 Inhibition or regression of xenograft tumor–growth by minicell delivery of shRNA or chemotherapeutic drug and reversal of multidrug resistance *in vivo* by sequential treatment with targeted, sh*MDR1*-containing minicells followed by targeted, chemotherapeutic drug-containing minicells. All minicell doses were administered intravenously in nude mice with 10^9 minicells per dose. The concentrations of drugs or shRNAs administered per dose in 10^9 minicells include (**a**) ~10^{11} copies of shRNA, (**b**) ~0.8 μg doxorubicin and (**c**) ~80 ng irinotecan. Free drugs were administered at 240 μg and 150 μg of irinotecan and doxorubicin, respectively. The days of treatment administration of the various minicells are shown below the *x*-axis. Error bars indicate ± s.e.m. (**a**) Drug resistant Caco-2/MDR1 xenografts ($n = 6$/group) were treated with ^{EGFR}minicells$_{shMDR1}$ followed by ^{EGFR}minicells$_{irinotecan}$ on days shown below the *x*-axis, which resulted in significant antitumor effects ($P < 0.0001$ versus all controls on day 32). Controls were untreated (saline) or were administered free irinotecan, or EGFR-targeted irinotecan- or sh*MDR1*-containing minicells, or EGFR-targeted sh*MDR1*-containing minicells followed by free irinotecan. (**b**) Kaplan-Meier survival analysis over 47 d of the animals treated in **a**, showing 100% survival only in the mice receiving the sequential treatment of ^{EGFR}minicells$_{shMDR1}$ followed by ^{EGFR}minicells$_{irinotecan}$ (**a**, G6). (**c**) The ability of sequential *MDR1* knockdown by ^{EGFR}minicells$_{shMDR1}$ followed by free doxorubicin or doxorubicin packaged in targeted minicells to suppress tumor growth was evaluated in mice bearing MDA-MB-468/MDR1 breast cancer xenografts ($n = 6$ per group). Drug resistance is evident from the continued tumor growth in the animals that received free doxorubicin (G2). Reversal of drug resistance was only observed in the animals given ^{EGFR}minicells$_{shMDR1}$ to suppress MDR1 expression, with the most marked antitumor effects being observed in those given sequential ^{EGFR}minicells$_{shMDR1}$ and then ^{EGFR}minicells$_{Dox}$ (G8 versus G1 or G2, $P < 0.0001$; G8 versus G7, $P < 0.0001$ at day 42).

Minicell delivery of si/shRNA *in vivo* and immune responses

We next investigated whether receptor-targeted minicells packaged with shRNA-encoding plasmid DNA or siRNA had antitumor effects in human cancer xenografts in mice.

Mice bearing colon cancer xenografts were administered intravenously specifically- (anti-EGFR) or nonspecifically- (anti-CD33) targeted minicells packaged with either si*PLK1*, si*KSP* or si*CDK1*. Compared with untreated mice (**Fig. 4a**), tumor growth was unchanged in animals that received nonspecifically targeted minicells or specifically targeted packaged with scrambled siRNA (^{EGFR}minicells$_{siNonsense}$) (G2 to G5 in **Fig. 4a**). In contrast, ^{EGFR}minicells$_{siPLK1}$, ^{EGFR}minicells$_{siKSP}$ or ^{EGFR}minicells$_{siCDK1}$ treatments (G6 to G8 in **Fig. 4a**) produced highly significant tumor growth inhibition ($P < 0.0007$, $P < 0.0005$ and $P < 0.0001$ for G6, G7 and G8 versus G1+G5, respectively). Failure to observe inhibition of tumor growth with nonspecifically targeted minicells carrying the same siRNAs indicates that BsAb-mediated targeting is essential.

To determine if targeted siRNA delivery via minicells effects knockdown of the targeted mRNA and protein *in vivo*, we repeated the HCT116 xenograft in additional mice and treated with ^{EGFR}minicells$_{siPLK1}$ and controls ^{EGFR}minicells$_{siNonsense}$ or saline. The tumor mass from each mouse was excised 4 h and 24 h after the last minicell dose and the extracted RNA was analyzed using real-time PCR for *PLK1* and *GAPDH* (control) mRNA expression. After 4 h and 24 h, the xenografts treated with ^{EGFR}minicells$_{siPLK1}$ exhibited ~24% and ~62% knockdown (**Fig. 4b**) of *PLK1* mRNA, respectively. In contrast, *PLK1* mRNA levels remained unchanged in mice treated with ^{EGFR}minicells$_{siNonsense}$. Analysis of total protein from each tumor mass, when processed by western blot analysis using anti-PLK1 monoclonal antibody, showed that, when compared with the saline-treated controls, at 4 h and 24 h there was clear knockdown of PLK1 in mice treated with ^{EGFR}minicells$_{siPLK1}$, but not in those treated with ^{EGFR}minicells$_{siNonsense}$ (**Fig. 4b**).

There is considerable debate surrounding the issue of the ability of nanoparticles to pass through the tumor-associated leaky vasculature and move within the tumor microenvironment to target many tumor cells. The distribution of the 400-nm minicells in the tumor has not yet been determined and needs to be elucidated before conclusions can be drawn concerning how the si/shRNA is able to reach sufficient tumor cells to inhibit tumor growth.

We next sought to evaluate the relative antitumor efficacy of minicell-mediated inhibition of proteins required for cell proliferation, such as KSP, as compared to the cytotoxic effects of the minicell-delivered chemotherapeutics doxorubicin (Dox) and paclitaxel (Pac), as demonstrated previously[9]. We treated mice bearing xenografts of human breast cancer cells (MDA-MB-468) with EGFR-targeted minicells containing doxorubicin, paclitaxel, both drugs, si*KSP* or sh*KSP*. Compared to untreated animals, all five treatments produced similar highly significant ($P < 0.0001$ in each case) levels of tumor stabilization (**Fig. 4c**,**d**). Treatment with minicell-delivered chemotherapeutics required less frequent dosing than needed for minicell-mediated siRNA delivery, most likely owing to the higher potency of cytotoxic drugs relative to knockdown of proteins required for cell division (**Fig. 4c**,**d**).

Recent studies[20] have questioned whether the antitumor effects of si/shRNA, as demonstrated in **Figure 4a**,**c**, result from specific knockdown of target mRNA or are instead nonspecific and merely due to siRNA-mediated activation of the innate immune response[21]. To address this issue, the HCT116 xenograft experiment was repeated with mice being treated with ^{EGFR}minicells$_{siPLK1}$, ^{EGFR}minicells$_{siNonsense}$ or saline (controls). Treatments were administered four times, 24 h apart, to mimic the treatments administered in the antitumor efficacy experiments (**Fig. 4a**,**c**). We euthanized groups of mice 4 h (early response) and 24 h (late response) after treatment and serum was collected and assayed for mouse and human type I and

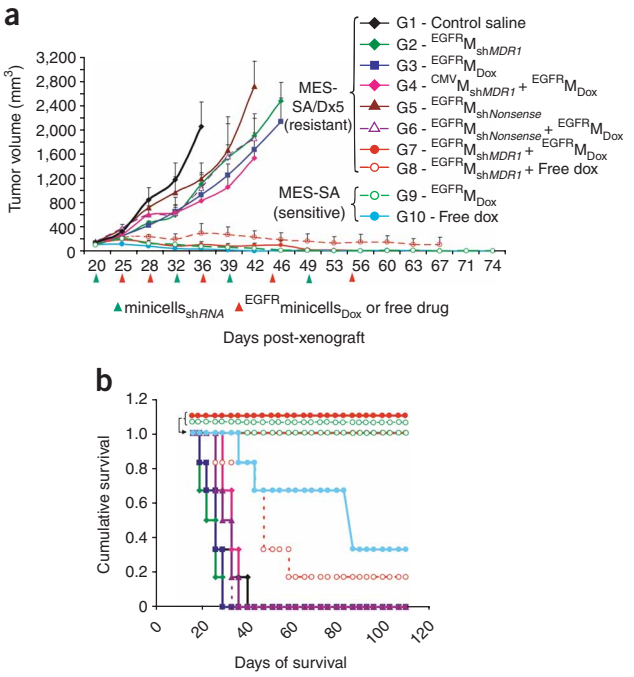

Figure 6 Reversal of multidrug resistance in MDR1-overexpressing aggressive uterine cancer xenografts with complete survival of mice administered dual sequential treatments. All minicell doses were administered intravenously in nude mice with 10^9 minicells per dose. The concentrations of doxorubicin or shRNAs administered per dose in 10^9 minicells were (**a**) ~10^{11} copies of shRNA and (**b**) ~0.8 μg doxorubicin. Free doxorubicin was administered at 150 μg/dose. The days of treatment administration of the various minicells are shown below the *x*-axis. Error bars indicate ± s.e.m. (**a**) Ability of sequential *MDR1* knockdown by ^{EGFR}minicells$_{shMDR1}$ followed by free doxorubicin or packaged in EGFR-targeted minicells to inhibit tumor growth in nude mice ($n = 6$/group) bearing a highly aggressive human uterine cancer cell (MES-SA/Dx5) xenograft that markedly overexpresses MDR1 (**Fig. 3c**). Controls (G1–G6) were untreated (G1, saline) or were given the treatments indicated. Responses to treatment with only the same doses, as above, of free doxorubicin, or EGFR-targeted, doxorubicin-containing minicells, were also evaluated in mice with doxorubicin-sensitive MES-SA uterine cancer cell xenografts. These cells did not constitutively express MDR1 (**Fig. 3c**). Note the highly significant ($P < 0.000$ for G1–G6 versus G7–G10) and persistent tumor growth suppression in groups G7–G10. sh*Nonsense* indicates short hairpin RNA with a scrambled sequence. (**b**) Kaplan-Meier survival curve for the xenograft study in **a** continued for up to 110 d, showing complete survival only in the MES-SA/Dx5 mice receiving sequential ^{EGFR}minicells$_{shMDR1}$ and then ^{EGFR}minicells$_{Dox}$ treatments (G7) or, as expected, in mice with the doxorubicin-sensitive MES-SA xenograft treated with ^{EGFR}minicells$_{Dox}$ (G9). For clarity, the line at a cumulative survival of 1.0 was redrawn at the top to more clearly show the responses of both G7 and G9.

II interferon (IFN), and for inflammatory cytokines produced by cells of the immune system. These cytokines are elicited following siRNA delivery to mice[21].

Supplementary Figure 2 shows that at both time points, human interferon and cytokine levels were low (range of ~10 to ~30 pg/ml) and the levels elicited by ^{EGFR}minicells$_{siPLK1}$ were indistinguishable from those observed with saline or ^{EGFR}minicells$_{siNonsense}$. In contrast, mouse interferon and cytokine responses were higher (in the range of ~50–150 pg/ml for IFN-α, -β and -γ; ~300–1,200 pg/ml for tumor necrosis factor (TNF)-α; and ~10–100 pg/ml for interleukin (IL)-6). Both IFN-γ and IL-6 showed a spike at 4 h, but returned to baseline (saline control level) by 24 h. Moreover, the TNF-α response was greater at 24 h than at 4 h. However, there were no significant differences in any of the interferon or cytokine levels in mice treated with ^{EGFR}minicells$_{siPLK1}$, compared with ^{EGFR}minicells$_{siNonsense}$ (**Supplementary Fig. 2**). The substantial increase in mouse TNF-α and IL-6 at 24 h may be attributed to the minicell vector itself, as systemic administration of bacterial cells activates Toll-like receptors, resulting in TNF-α and IL-6 responses[22]. However, with minicell administrations in mice, these responses have been self-limiting, returning to baseline within ~24 h (for IL-6; **Supplementary Fig. 2**) to 48 h (data not shown), and have not resulted in toxicity to the mice.

These results indicate that the potent antitumor effects observed in mouse xenografts (**Fig. 4a**,**c**) are unlikely to be due to interferon or inflammatory cytokine responses, as treatment with EGFR-targeted si*Nonsense*-containing minicells did not produce any antitumor effects despite similar interferon and cytokine responses as those in mice treated with ^{EGFR}minicells$_{siPLK1}$.

Dual sequential treatment reverses drug resistance *in vivo*

To investigate whether dual minicell therapy, first to overcome drug resistance and then to inhibit tumor growth, is effective as an *in vivo* therapeutic approach, mice bearing Caco-2/MDR1 xenografts were treated with ^{EGFR}minicells$_{shMDR1}$ followed by either free irinotecan or ^{EGFR}minicells$_{irinotecan}$. In initial studies, we determined that the optimal time between treatment with siRNA- or shRNA-containing minicells to knock down *MDR1* expression, and then treatment with cytotoxic drug–containing minicells, was ~48 h and ~144 h for siRNA- and shRNA-containing minicells, respectively (**Supplementary Results** and **Supplementary Fig. 3a**,**b**).

Compared to all control groups, dual sequential treatment with ^{EGFR}minicells$_{shMDR1}$ followed by ^{EGFR}minicells$_{irinotecan}$ given on the days indicated markedly inhibited tumor growth (**Fig. 5a**; G6 versus all controls, $P < 0.0001$), despite the strong resistance of the xenografts to free irinotecan (G2). Kaplan-Meier analysis showed complete survival of the mice treated with the dual treatment procedure, whereas those in all other groups died early (**Fig. 5b**). This marked survival difference is especially striking in view of the administration of free irinotecan at 12 mg/kg per dose (~240 μg per mouse dose), in contrast with an equivalent minicell mouse dose of ~80 ng. This equates to ~3,000-fold less irinotecan being administered via minicell-mediated delivery. Similar results were obtained when ^{EGFR}minicells$_{irinotecan}$ was replaced with ^{EGFR}minicells$_{5\text{-}FU}$ (**Supplementary Fig. 4a**,**b**).

We also investigated the dual treatment procedure in xenografts established using a breast cancer cell variant (MDA-MB-468/MDR1) that is resistant to doxorubicin and constitutively expresses MDR1 (**Fig. 3c**). Mice were treated with ^{EGFR}minicells$_{shMDR1}$, followed by either ^{EGFR}minicells$_{Dox}$ or free doxorubicin. This dual sequential treatment was also highly effective in inhibiting tumor growth (**Fig. 5c**; G8 versus G1–G6; $P < 0.0001$). Treatment with ^{EGFR}minicells$_{shMDR1}$ followed by free doxorubicin (G7) also produced significant tumor growth inhibition (G7; $P < 0.0001$ for G7 versus G1 and G3–G6), but was not as effective as the dual minicell therapy. Doxorubicin resistance of the MDA-MB-468/MDR1 cells was not as strong as that of the Caco-2/MDR1 cells, which express higher levels of MDR1. Not surprisingly, therefore, some antitumor effects were evident with free doxorubicin treatment alone, and although significant ($P < 0.0248$ for G2 versus G1 and G3–G6), were not as marked as those observed with dual treatment. In these studies, ~150-fold less doxorubicin was administered per dose via minicells (1 μg) compared to without minicells, as free drug (150 μg).

In the above three xenograft studies, it would also be expected that dual treatment with ^{EGFR}minicells$_{shMDR1}$ followed by free drug should exhibit antitumor effects similar to those observed if both treatments were administered via minicells. However, this was only observed in the MDA-MB-468/MDR1 xenograft (**Fig. 5c**), likely because MDR1 overexpression is less marked in MDA-MB-468/MDR1 than in Caco-2/MDR1 cells (**Fig. 3c**). Drug resistance in mice bearing Caco-2/MDR1 xenografts is so robust that even after ^{EGFR}minicells$_{shMDR1}$-mediated MDR1 knockdown, the amount of free irinotecan or 5-FU required to kill tumor cells is sufficient to cause systemic toxicity. *In vitro*, however, where systemic toxicity is not an issue, Caco-2/MDR1 cells treated with ^{EGFR}minicells$_{shMDR1}$ followed by free drug show reversal of drug resistance and subsequent inhibition of cell proliferation (**Fig. 3d**).

shRNA delivery reverses drug resistance in an aggressive tumor

We next studied whether the dual treatment would also be effective for treating xenografts established using MES-SA/Dx5 human uterine cancer cells, a more aggressive multidrug-resistant tumor cell line. As a control, we also developed xenografts using MES-SA cells that are not resistant to multiple drugs, do not constitutively express MDR1 (**Fig. 3c**) and are sensitive to doxorubicin. These studies showed that dual treatment of MES-SA/Dx5 with ^{EGFR}minicells$_{shMDR1}$ followed by ^{EGFR}minicells$_{Dox}$ (**Fig. 6a**, G7) or free doxorubicin (**Fig. 6a**, G8) was highly effective ($P < 0.0001$ in both cases versus saline control) in reversing drug resistance. After ~70 d, there was no evidence of tumors in mice treated first with ^{EGFR}minicells$_{shMDR1}$ and then ^{EGFR}minicells$_{Dox}$ (G7). As expected, in animals with doxorubicin-sensitive control MES-SA cell xenografts, treatment with ^{EGFR}minicells$_{Dox}$ alone eliminated tumors by ~day 70 ($P < 0.0001$). None of the various control treatments showed any antitumor effects and the tumors grew aggressively, requiring euthanization of animals as early as 42 d after implantation. In this study, the survival of mice was evaluated for up to 110 d after tumor implantation. For the MES-SA/Dx5 xenografts, all six mice that received the dual treatment via minicells survived with no evidence of tumors (**Fig. 6b**). In contrast, mice from all other groups died early at the times shown. Mice treated with ^{EGFR}minicells$_{shMDR1}$ followed by free doxorubicin, (G8), which had demonstrated drug-resistance reversal, also died. This most likely results from the well-known toxicity of free doxorubicin. In animals with doxorubicin-sensitive MES-SA cell xenografts, treatment with ^{EGFR}minicells$_{Dox}$ also resulted in 100% survival (**Fig. 6b**), consistent with our previous observations[9].

DISCUSSION

We have developed a robust and versatile system for targeted *in vivo* delivery of si/shRNA using minicells—bacterially derived carriers with diameters of ~400 nm. The ability to package minicells with siRNAs with >80% efficiency is unexpected, considering that the large molecular weight (~14 kDa) and polyanionic character of double-stranded siRNAs are generally thought to limit their passage across membranes and thus, their entry into cells. Further studies will be required to elucidate the mechanisms by which minicells can be so readily loaded with double-stranded siRNA. Presumably, this occurs via specific protein channels, as the minicell membrane is primarily composed of phospholipids, lipopolysaccharides and proteins, and it is well recognized that siRNAs do not breach the phospholipid barrier[23].

The limited payload capacity of most carriers is a major limitation to the use of siRNA as a therapeutic. For example, antibodies[24] and aptamers[25] can carry ~10 and ~2,000 siRNA molecules per targeting agent, respectively[26]. In contrast, we show that minicells can carry at least ~12,000 siRNA molecules and ~100 copies of shRNA-encoding plasmid. Moreover, once packaged, siRNAs are stable, resistant to degradation by extrinisic RNases, and do not leak out of minicells. Further, si/shRNA-containing minicells can be specifically targeted to tumor-cell-surface proteins with BsAb and, as we show here, such specific targeting of minicells is essential to efficiently kill tumor cells.

Evaluation of the uptake and intracellular kinetics of minicell-delivered siRNA indicates that after endocytosis, the minicells traverse the well-established early and late endosomal pathways, terminating in acidified organelles, the lysosomes, where they are degraded and release their cargo. This was evident where fluorescent siRNA-containing minicells appeared to be endocytosed in substantial numbers by MES-SA/Dx5 tumor cells (**Fig. 2a**,**b**). Further, although lysosomal activity was minimal at early time points, most of the minicells appeared inside lysosomes within 4 h and 8 h after administration. By 24 h, lysosomal activity returned to normal, and fluorescent siRNA was distributed throughout the cytoplasm. These findings indicate that a substantial number of functionally intact siRNA molecules escape from the lysosomal compartment into the cytosol.

Our studies also show that substantial target-protein knockdown, potent inhibition of tumor cell proliferation, induction of G2 arrest and apoptosis and highly significant inhibition of tumor xenografts *in vivo*, can all be triggered with minicells targeted to tumors via BsAb that are packaged with siRNAs directed against critical cell cycle–associated proteins, such as PLK1, KSP or CDK1. Moreover, in studies of mice with a breast cancer xenograft, the relative antitumor efficacy of targeted minicell-mediated delivery of si*KSP* or sh*KSP* was similar to that observed with minicell-mediated delivery of the cytotoxic drugs doxorubicin and paclitaxel. This is of interest, as a single minicell carries ~830,000 and ~21,000 molecules of doxorubicin and paclitaxel, respectively[9], compared to only ~12,000 molecules of siRNA or ~100 copies of shRNA-encoding plasmid.

Of considerable interest was the observation that tumor-cell drug resistance due to overexpression of MDR1 (used here as a model marker of drug resistance), could be reversed by first treating the tumor cells with EGFR-targeted minicells packaged with sh*MDR1* to initially reduce levels of MDR1. This resulted in the cells becoming sensitive to minicell-delivered cytotoxic therapy and indicates that the same tumor cells were not only receptive to at least two waves of minicell therapy, each involving different payloads, but also that their endocytosis and intracellular processing machinery remains competent after the first wave of minicell delivery.

Drug resistance could be reversed even in animals with xenografts established from human uterine cancer cells that markedly overexpress MDR1. Once reversal was established, these tumors became sensitive (**Fig. 6a**) to chemotherapeutic drugs, enabling complete survival for at least 110 d (**Fig. 6b**).

Nonspecific activation of immunological and/or inflammatory pathways by bacterial products cannot account for the antitumor effects observed in our studies, as in no instance did nontargeted or nonspecifically targeted minicells, with or without packaged siRNA/shRNA, inhibit tumor growth. Importantly, minicells were well-tolerated with no adverse side effects or deaths in any of the actively treated animals, despite repeat dosing. Extensive evaluation of human and mouse inflammatory cytokine and IFN responses in mice treated with ^{EGFR}minicells$_{siPLK1}$ or ^{EGFR}minicells$_{siNonsense}$ also showed no major differences in the immune responses elicited by these two treatments. Nevertheless, given that minicells are of bacterial origin, caution with their parenteral administration is warranted, as bacterial products can elicit potent inflammatory responses activated by Toll-like receptors[27]. Although our previous *in vivo* studies[9] revealed only very weak immunogenicity of the dominant minicell surface–exposed antigen,

O-polysaccharide, and that repeat i.v. administration did not result in immune-exclusion of subsequent doses, extensive evaluation of immunogenicity is needed to determine the nature of humoral and cellular immunity to minicells both in tumor-bearing and naïve animals.

Although other nanoparticles being developed for targeted drug-delivery show some ability to directly overcome MDR-mediated drug resistance[28], our findings indicate that multidrug resistance is a complex phenomenon that depends on several variables. These include the level of MDR expression, which can vary widely in different tumor cell lines, and the differing modes of action of cytotoxic drugs. As a result, in the absence of MDR knockdown, even drug delivery via nanoparticles may be limited in its ability to affect tumor stabilization or regression.

Nano-sized drug delivery systems, such as immunoliposomes, are currently believed to target tumors by an initial passive process termed the 'enhanced permeability and retention effect'. This involves extravasation from the leaky vasculature (pore sizes 200–1.2 μm[29,30]) that supports the tumor microenvironment and is followed by active targeting via cancer cell-surface receptor engagement and endocytosis[31]. Similar considerations may underlie the potent antitumor efficacy of minicell-based si/shRNA delivery.

An important feature of targeted minicell-mediated si/shRNA and drug-delivery is its ability to achieve inhibition or regression of tumor growth with delivery of amounts of therapeutic agents that are markedly smaller than those required with systemic delivery of free drugs. For example, with delivery of targeted minicells carrying irinotecan, 5-FU or doxorubicin, tumor growth-inhibition was substantially more marked than with the administration of ~3,000-fold, ~25,000-fold and ~150-fold higher amounts of their respective free-drugs. This remarkable efficacy is likely due to both the large payload capacity of minicells and the ability to deliver them directly to the intracellular environment of tumor cells.

METHODS

Methods and any associated references are available in the online version of the paper at http://www.nature.com/naturebiotechnology/.

Note: Supplementary information is available on the Nature Biotechnology website.

ACKNOWLEDGMENTS

This work was supported in part by a Commercial Ready Grant from AusIndustry, Australia. We appreciate the assistance of R.P. Paulin, G. Al Bakri, M. Harrison and R. Emira in minicell purification. We thank S. Pattison and N. Grimes for technical assistance. We are grateful to S. Friend, L. Sepp-Lorenzino and W. Tao (Merck & Co., West Point, PA, USA) for the permission to publish the work associated with the kinesin spindle protein (KSP) siRNA sequence. The authors dedicate this paper to R.M.G.'s mother, who died of metastatic renal cell carcinoma on August 5, 2008.

AUTHOR CONTRIBUTIONS

H.B. and J.A.M. conceived the project and co-invented the minicell delivery technology. They designed the experiments and analyzed the data and wrote the manuscript. J.A.M. also carried out critical breakthrough experiments. N.B.A.-M. constructed the shRNA plasmids, packaged the siRNA into minicells and carried out the quantification studies. J.M-W. and S.W. packaged drugs into minicells and performed *in vitro* transfection studies and *in vivo* xenograft studies. I.S., K.K. and C.P. carried out intracellular kinetic studies and established target knockdown *in vivo*. S.T.P. performed the immune response studies and V.N.B. constructed the bispecific antibodies and targeted the minicells. L.P. estimated minicell packaged drug quantification. R.M.G. and B.S. provided helpful discussion and R.M.G. also assisted in writing the manuscript.

COMPETING INTERESTS STATEMENT

The authors declare competing financial interests: details accompany the full-text HTML version of the paper at http://www.nature.com/naturebiotechnology/.

Published online at http://www.nature.com/naturebiotechnology/
Reprints and permissions information is available online at http://npg.nature.com/reprintsandpermissions/

1. Fire, A. *et al.* Potent and specific genetic interference by double-stranded RNA in *Caenorhabditis elegans*. *Nature* **391**, 806–811 (1998).
2. Aagaard, L. & Rossi, J.J. RNAi therapeutics: principles, prospects and challenges. *Adv. Drug Deliv. Rev.* **59**, 75–86 (2007).
3. Kawakami, S. & Hashida, M. Targeted delivery systems of small interfering RNA by systemic administration. *Drug Metab. Pharmacokinet.* **22**, 142–151 (2007).
4. Bartlett, D.W. & Davis, M.E. Impact of tumor-specific targeting and dosing schedule on tumor growth inhibition after intravenous administration of siRNA-containing nanoparticles. *Biotechnol. Bioeng.* **99**, 975–985 (2008).
5. McNamara, J.O. *et al.* Cell type-specific delivery of siRNAs with aptamer-siRNA chimeras. *Nat. Biotechnol.* **24**, 1005–1015 (2006).
6. Pirollo, K.F. & Chang, E.H. Targeted delivery of small interfering RNA: approaching effective cancer therapies. *Cancer Res.* **68**, 1247–1250 (2008).
7. Sorensen, D.R., Leirdal, M. & Sioud, M. Gene silencing by systemic delivery of synthetic siRNAs in adult mice. *J. Mol. Biol.* **327**, 761–766 (2003).
8. De Boer, P.A., Crossley, R.E. & Rothfield, L.I. A division inhibitor and a topological specificity factor coded for by the minicell locus determine proper placement of the division septum in *E. coli*. *Cell* **56**, 641–649 (1989).
9. MacDiarmid, J.A. *et al.* Bacterially derived 400 nm particles for encapsulation and cancer cell targeting of chemotherapeutics. *Cancer Cell* **11**, 431–445 (2007).
10. MacDiarmid, J.A., Madrid-Weiss, J., Amaro-Mugridge, N.B., Phillips, L. & Brahmbhatt, H. Bacterially-derived nanocells for tumor-targeted delivery of chemotherapeutics and cell cycle inhibitors. *Cell Cycle* **6**, 2099–2105 (2007).
11. Heidel, J.D. *et al.* Potent siRNA inhibitors of ribonucleotide reductase subunit RRM2 reduce cell proliferation *in vitro* and *in vivo*. *Clin. Cancer Res.* **13**, 2207–2215 (2007).
12. Villares, G.J. *et al.* Targeting melanoma growth and metastasis with systemic delivery of liposome-incorporated protease-activated receptor-1 small interfering RNA. *Cancer Res.* **68**, 9078–9086 (2008).
13. Strebhardt, K. & Ullrich, A. Targeting polo-like kinase 1 for cancer therapy. *Nat. Rev. Cancer* **6**, 321–330 (2006).
14. Tao, W. *et al.* Induction of apoptosis by an inhibitor of the mitotic kinesin KSP requires both activation of the spindle assembly checkpoint and mitotic slippage. *Cancer Cell* **8**, 49–59 (2005).
15. Nigg, E.A. Mitotic kinases as regulators of cell division and its checkpoints. *Nat. Rev. Mol. Cell Biol.* **2**, 21–32 (2001).
16. Kaszubiak, A., Holm, P.S. & Lage, H. Overcoming the Classical Multidrug Resistance Phenotype by Adenoviral Delivery of anti-MDR1 Short Hairpin RNAs and Ribozymes. *Int. J. Oncol.* **31**, 419–430 (2007).
17. Gottesman, M.M., Fojo, T. & Bates, S.E. Multidrug resistance in cancer: role of ATP-dependent transporters. *Nat. Rev. Cancer* **2**, 48–58 (2002).
18. Meagher, R.B., Tait, R.C., Betlach, M. & Boyer, H.W. Protein expression in *E. coli* minicells by recombinant plasmids. *Cell* **10**, 521–536 (1977).
19. El-Rayes, B.F. & LoRusso, P.M. Targeting the epidermal growth factor receptor. *Br. J. Cancer* **91**, 418–424 (2004).
20. Poeck, H. *et al.* 5′-triphosphate-siRNA: turning gene silencing and Rig-I activation against melanoma. *Nat. Med.* **14**, 1256–1263 (2007).
21. Robbins, M. *et al.* Misinterpreting the therapeutic effects of small interfering RNA caused by immune stimulation. *Hum. Gene Ther.* **19**, 991–999 (2008).
22. Wilson, M., Seymour, R. & Henderson, B. Bacterial perturbation of cytokine networks. *Infect. Immun.* **66**, 2401–2419 (1998).
23. Meade, B.R. & Dowdy, S.F. Enhancing the cellular uptake of siRNA duplexes following noncovalent packaging with protein transduction domain peptides. *Adv. Drug Deliv. Rev.* **60**, 530–536 (2008).
24. Song, E. *et al.* Antibody mediated *in vivo* delivery of small interfering RNAs via cell-surface receptors. *Nat. Biotechnol.* **23**, 709–717 (2005).
25. McNamara, J.O. II *et al.* Cell type-specific delivery of siRNAs with aptamer-siRNA chimeras. *Nat. Biotechnol.* **24**, 1005–1015 (2006).
26. Bartlett, D.W. & Davis, M.E. Physicochemical and biological characterization of targeted, nucleic acid-containing nanoparticles. *Bioconjug. Chem.* **18**, 456–468 (2007).
27. Akira, S. & Takeda, K. Toll-like receptor signaling. *Nat. Rev. Immunol.* **4**, 499–511 (2004).
28. Mayer, L.D. & Shabbits, J.A. The role for liposomal drug delivery in molecular and pharmacological strategies to overcome multidrug resistance. *Cancer Metastasis Rev.* **20**, 87–93 (2001).
29. Hobbs, S.K. *et al.* Regulation of transport pathways in tumor vessels: role of tumor type and microenvironment. *Proc. Natl. Acad. Sci. USA* **95**, 4607–4612 (1998).
30. Yuan, F. *et al.* Microvascular permeability and interstitial penetration of sterically stabilized (stealth) liposomes in a human tumor xenograft. *Cancer Res.* **54**, 3352–3356 (1994).
31. Mamot, C. *et al.* Epidermal growth factor receptor (EGFR)-targeted immunoliposomes mediate specific and efficient drug delivery to EGFR- and EGFRvIII-overexpressing tumor cells. *Cancer Res.* **63**, 3154–3161 (2003).

ONLINE METHODS

Reagents, minicell generation, purification, enumeration and si/shRNA-packaging. Minicells were produced and purified from an *S. typhimurium* *min*CDE$^-$ strain as previously described[9]. The siRNA sequences used in this study include; (i) si*PLK1* (sense strand, 5′-GGUGGAUGUGUGGUCCAU UdTdT-3′ and anti-sense strand, 5′-AAUGGACCACACAUCCACCdTdC-3′; validated sequence from Ambion). The target sequence, 5′-GAGGTGGATG TGTGGTCCATT-3′, is found between bases 746 and 764 of the *PLK1* gene (accession number NM_005030). (ii) si*CDK1* (sense strand, 5′-GGUUAUAU CUCAUCUUUGAUU-3′ and anti-sense strand 5′-UCAAAGAUGAGAUAUAA CCUU-3′; validated sequence from Dharmacon). The target sequence, 5′-GGT TATATCTCATCTTTGA-3′, is found between bases 237 and 255 of the *Cdk1* gene (accession number NM_033379). (iii) si*KSP* (sense strand, 5′-CUGAA GACCUGAAGACAAUdTdT-3′ and the anti-sense strand is 5′-AUUGTCUU CAGGUCUUCAGdTdT-3′). The target sequence, 5′-AACTGAAGACCTGAA GACAAT-3′[32] (Ambion positive control) is found between bases 2261-2281 (accession number NM_004523). (iv) si*Nonsense* (sense strand, 5′-UCAGU CACGUUAAUGGUCGdTdT-3′ and anti-sense is 5′-CGACCAUUAACGUGA CUGAdTdT-3′; validated sequence from Imgenex). The scrambled sequence is, 5′-TCAGTCACGTTAATGGTCGTT-3′.

siRNAs were manufactured by Qiagen and lyophilized siRNAs were resuspended in Qiagen siRNA resuspension buffer to give a 20 μM stock solution. siRNA solutions were heated to 90 °C for 1 min followed by 37 °C for 1 h. Fluorescently-tagged siRNAs for *PLK1, KSP* and *MDR1* were synthesized (Qiagen) with a 3′ AF488 or AF555 or AF647 modification. siRNAs were degraded by incubating with RNase cocktail (Ambion) containing RNase A and RNase T1, as recommended by the manufacturer.

siRNA packaging in minicells was carried out as follows: 10^{10} minicells were washed once with 1 ml of RNase-free 1× PBS pH 7.4, and centrifuged at 16,100*g* for 6.5 min. The supernatant was discarded and the minicell pellet was resuspended in a 1 ml solution of RNase-free 1× PBS pH 4.0 with siRNA to a final concentration of 1 μM. The solution was incubated overnight at 37 °C with gentle mixing. Loaded minicells were washed twice in 1 ml of RNase-free 1× PBS pH 7.4 and centrifuged as above. After the second wash and aspiration of the supernatant, minicells were subjected to fluorescence microscopy, or targeted by incubation with 5 μg of anti-O-polysaccharide/anti-EGFR BsAb for 1 h at 24 °C as previously described[9]. siRNA was resolved by 20% SDS-PAGE and stained with ethidium bromide.

To quantitate siRNAs packaged in minicells, siRNA was extracted from loaded minicells (in triplicate) using the TaqMan MicroRNA Cells-to-CT kit (Applied Biosystems) according to the manufacturer's instructions. siRNAs were reverse transcribed using a stem-loop primer to generate cDNA and real-time PCR was carried out using an siRNA-specific forward primer, a reverse primer and a Taqman probe, as detailed in Online Methods.

The vector for shRNA directed against *MDR*1 was made by cloning shRNA oligonucleotides to the target sequence 5′-AAGAAACCAACTGTCAG TGTA-3′[33] (bases 506–526 accession number NM_000927) into the shRNA expression plasmid, IMG-800 (pSuppressorNeo, Imgenex) in which expression is under the control of the U6 promoter. Sense and anti-sense shRNA oligonucleotides were designed, annealed and cloned according to manufacturer's specifications. For plasmid construction, two complementary oligonucleotides containing human *MDR1* sequences were synthesized (Sigma) and annealed to generate double-stranded DNA, which was cloned into the *Sal*I and *Xba*I cloning sites of IMG-800. All positive clones were confirmed by DNA sequencing. The recombinant plasmids were transformed into the *S. typhimurium* *min*CDE$^-$ strain and resulting clones were purified. Recombinant minicells carrying shRNA-encoding plasmids were generated following the transformation of the minicell-producing bacterial strain *S. typhimurium* *min*CDE$^-$, with the plasmids. Plasmid DNA segregated into the minicell cytoplasm during asymmetric septum formation and recombinant minicells were purified as described above.

BsAb construction, fluorescence tagging and tumor targeting. BsAb was constructed by linking an anti-*S. typhimurium* O-polysaccharide MAb (IgG1; Biodesign) and a mouse MAb directed against a cancer cell-surface receptor for example, anti-human EGFR (IgG2a; Calbiochem), as described[9]. Nonspecifically targeted BsAb carried an anti-CD33 mAb (IgG1; Abcam) or anti-CMV mAb (IgG2a; DakoCytomation). The two antibodies were cross-linked as previously detailed[9], via their Fc regions using purified recombinant protein A/G (Pierce Biotechnology), which results in BsAb as well as multimeric complexes. This linkage blocks the Fc regions of both antibodies thus limiting immunological reactivity to these regions. BsAb was incubated with minicells for 1 h at 25 °C to enable binding to the minicell-surface O-polysaccharide. Excess unbound BsAb was removed by filtration through 0.2 μm filter (PALL). Approximately 5 μg of the BsAb complex was sufficient to saturate 10^9 minicells. AF488 and AF647-labeling of BsAbs and anti-O-polysaccharide mAb was carried out according to the manufacturer's instructions (Invitrogen/Molecular Probes). The dissociation constant of anti-O-polysaccharide mAb was determined as described in **Supplementary Results**.

Minicell quantification and cell cycle analysis. Minicells were quantitated based on SYTO-9 fluorescence, as previously described[9]. Briefly, $\sim 2 \times 10^6$ minicells (estimated using measurements at OD_{600nm}) were incubated with 6 μM solution of SYTO-9 (Molecular Probes) and FACS calibration beads (Molecular Probes) for 10 min. FACS analysis was carried out using an FC500 Beckman Coulter Flow Cytometer detecting at FL1 channel and the CXP software (Beckman Coulter). Because the intrinsic fluorescence of drugs or siRNA packaged in minicells could interfere with SYTO-9 fluorescence, minicells were also quantitated using another method based on the fluorescence of AF647-tagged anti-O-polysaccharide mAb bound to minicell-surface O-polysaccharides. Briefly, AF647 (Invitrogen; excitation at 650 nm, emission at 668 nm) was conjugated to an anti-O-polysaccharide mAb (Biodesign) according to the manufacturer's instructions. The resulting AF647-tagged mAb ($\sim$500 ng) was then incubated at 25 °C with $\sim 10^7$ minicells in PBS for 20 min. After three washes in PBS, the fluorescent minicells were then quantitated by FACS as mentioned above using the FL4 channel.

Cell cycle analysis was performed using the propidium iodide staining method. Briefly, $\sim 10^6$ cells/ml were washed twice with cold PBS and fixed in 70% ethanol for 2 h at −20 °C. Immediately before analysis, the cells were washed with PBS and stained with a solution containing 40 μg/ml propidium iodide and 0.2 mg/ml RNase A for 30 min. at 25 °C. The stained cells were analyzed using FACS with detection at FL3 channel.

Cancer cell lines, transfection with minicells, cell proliferation assay and protein immunoblotting. MES-SA (human uterine sarcoma), MES-SA/Dx5 (multidrug resistant variant of MES-SA), HCT116 (human colorectal carcinoma), Caco-2 (human colonic adenocarcinoma), MDA-MB-468 (human breast adenocarcinoma) cell lines (ATCC) and Caco-2/MDR1 (P-gp expressing variant of Caco-2), MDA-MB-468/MDR1 (P-gp expressing variant of MDA-MB-468), were maintained in RPMI-1640 medium (Lonza) supplemented with 10% FCS (Lonza) and 100 units/ml of penicillin and streptomycin (Lonza).

The MTT cell proliferation inhibition assay was carried out as follows: 5×10^5 HCT116 or Caco-2/MDR1 cells were plated on coverslips in 6-well plates 1 d before transfection. Medium was removed from wells and 600 μl of complete RPMI medium containing 5×10^9 minicells were added into each well, resulting in minicell:cell transfection ratio of 10,000:1. Plates were incubated for 2 h at 37 °C, the transfection mixture was removed, cells were washed twice in PBS and fresh growth medium added. The CellTiter 96 Aqueous One Solution Cell Proliferation Assay (MTT; Promega) was used to determine cell survival according to the manufacturer's instructions.

Protein immunoblotting was carried out as follows: cells were lysed in lysis buffer comprising 50 mM Tris, pH 8; 150 mM NaCl; 10% glycerol; 0.2% Triton ×100; 1 mM DTT; phosphatase inhibitor cocktail I (AG Scientific) and II (Calbiochem) and protease inhibitor cocktail (Roche). The protein concentration (DC protein assay; BioRad) of clarified cell lysates was determined and 50 μg of total protein per well was resolved by 4–12% SDS-PAGE (Invitrogen) and transferred to PVDF membranes, blocked with 5% skim milk for 1 h at 25 °C and then incubated with anti-PLK1 mouse mAb (Abcam) or anti-P-gp mAb (Abcam) and anti-β-actin mAb (Chemicon), washed and developed using chemiluminescence ECL plus detection reagents (Amersham Biosciences).

Drug packaging in minicells, drug extraction and quantification. Drug packaging in minicells, extraction and quantification was carried out as

doi:10.1038/nbt.1547

previously described[9]. Briefly, chemotherapeutic drugs, doxorubicin (Sigma) and paclitaxel (Calbiochem) were dissolved in sterile physiological saline and in 50:50 (vol/vol) Cremophor EL:ethanol, respectively. Paclitaxel solution was diluted 1:5 in 0.9% saline, immediately before injection. Purified minicells (3×10^{10}) were incubated overnight at 37 °C, with 100 μg/ml of either doxorubicin, paclitaxel, irinotecan (Aventis) or 5-FU (Sigma). Doxorubicin, irinotecan and 5-FU were dissolved in sterile buffered saline gelatin (BSG), and paclitaxel was dissolved in BSG with 15% ethanol. Post-drug loading into minicells, excess drug was removed by Amicon stirred-cell ultrafiltration (Millipore; 300 kDa cut-off filter) with six washes of sterile BSG.

Drug extraction from packaged minicells was carried out as described[9]. Briefly, it involved five cycles of vortexing and sonication in the presence of 97 mM HCl-isopropyl alcohol (HCl-IPA) and water. After centrifugation at 16,100*g* for 5 min to pellet debris, the supernatants were harvested for drug quantification.

Doxorubicin and irinotecan extracted from minicells were quantitated based by HPLC-fluorescence peak analyses, as previously described for doxorubicin[9,34,35] and irinotecan[36]. HPLC analysis was performed on a Shimadzu 10AVP system incorporating a RF-10A XL fluorescence detector. Extracted paclitaxel was quantitated using UV-Vis absorbance at 228 nm, as described[37,38]. Extracted 5-FU was quantitated by LC-MS using a Thermo Finnigan MS (University of Sydney) run in negative mode, as previously described[9].

Fluorescence and confocal microscopy. Fluorescence microscopy images of minicells were captured using a Leica DMLB fluorescence microscope with an Olympus DP70 camera and DP controller/camera software. Images showing the minicell-cancer cell interactions were captured using a IX81 confocal microscope (Olympus) and CellR software as described previously[9].

Tumor xenograft and *in vivo* protein/mRNA knockdown studies in nude mice. Athymic (*nu/nu*) mice (4–6 weeks old) were purchased from the Animal Resources Centre (Perth Western Australia) and all animal experiments were performed in compliance with National Health and Medical Research Council, Australia guidelines for the care and use of laboratory animals, and with EnGeneIC Animal Ethics Committee approval. Caco-2/MDR1, HCT116, MDA-MB-468/MDR1, MES-SA, MES-SA/Dx5 human tumor cell lines were cultured and 1.5×10^6 cells in 50 μl serum-free media together with 50 μl growth factor reduced matrigel (BD Biosciences) and injected subcutaneously between the shoulder blades. Tumor volume (mm^3) was determined by measuring length (l) and width (w) and calculating volume ($V = lw^2/2$) as described[39]. Experimental and control treatments were carried out once the tumor volumes were between 150 and 200 mm^3, at which time the tumor mass was clearly palpable and vascularized, as determined following excision and histological examination of tumors. Mice were randomized to different groups before starting the various treatments. All tumor volume-measurements were performed by an investigator blinded to the treatments administered. Kaplan Meier analyses were used to assess survival. Statistical analysis was performed by analysis of variance (ANOVA), with $P < 0.05$ being considered significant.

Total RNA and protein were extracted from xenografted tumors following tumor excision and snap freezing in liquid nitrogen. Tumors were sonicated on ice, homogenized and one third of the homogenate was used for RNA extraction and the remaining for protein extraction. RNA was extracted using the Qiazol lysis reagent (Qiagen) and quantitated spectrophotometrically at OD_{260nm}. cDNA was synthesized with random hexamers using Superscript III Reverse transcriptase kit according to the manufacturers instructions (Invitrogen). Real-time PCR was carried out as described in **Supplementary Methods** and the results for *PLK1* amplification were normalized against *GAPDH* amplification.

Molecular Biology protocols. Plasmid DNA was purified using the Qiaprep Spin Miniprep Kit (Qiagen). All restriction and modification enzymes were from Promega or Roche, except for Deep Vent DNA Polymerase, which was purchased from New England Biolabs. PCR primers were synthesized and purchased from Sigma-Genosys. Standard molecular biology protocols followed were as described[40,41].

Minicell purification and enumeration. Minicells were produced and purified from an *S. typhimurium minCDE*$^-$ strain as previously described[9].

siRNA quantification. Quantification of siRNA packaged into minicells involved extraction of siRNA from loaded minicells, reverse transcription using a stem-loop primer that binds to the siRNA to make cDNA, and then real-time PCR of the cDNA products, using an siRNA-specific forward primer, a reverse primer and TaqMan probe, as described previously[42,43]. siRNA was extracted from loaded and empty (control) minicells (in triplicate) using the TaqMan MicroRNA Cells-to-CT kit (Applied Biosystems) according to the manufacturer's instructions. The sequences used for the qPCR were as follows; (i) siRNA sequence for MDR1 (5′-GAGCUUAACACCCGACUUACATT-3′; Ambion), (ii) corresponding stemloop primer (5′-GTCGTATCCAGTGCAG GGTCCGAGGTATTCGCACTGGATACGACAATGTA-3′) for the reverse transcriptase reaction, (iii) forward primer (5′-GATGCTTAACACCCGACT-3′), (iv) reverse primer (5′-GTGCAGGGTCCGAGGT-3′), and (v) TaqMan probe [(6-fam) 5′ cac+Tg+Ga+Ta+Cga+Caa+Tgta 3′ (BHQ1)]. The forward and reverse primers were designed following TaqMan assay guidelines to have the same melting temperature (Tm) of 54 °C. The TaqMan probe was designed using LNA (locked nucleic acid) bases which raise the Tm of the probe without having to increase the length significantly. Primers and probes were manufactured by Sigma Proligo and resuspended in RNase-free water to 50 μM and stored at –20 °C. cDNA extension was carried out on the lysis products using the reverse transcriptase Superscript III (Invitrogen). Eight μl of lysis reaction sample were mixed with 2 pmoles of stem-loop primer and the mixture heated to 85 °C for 2 min. The 33 samples were snap chilled on ice and then the reaction was made up to 20 μl with 1 μl of 0.1M DTT, 10U RNase inhibitor (Roche), 1 μl of 10 mM dNTPs (Invitrogen), 4 μl 5× first strand buffer and 1 μl of 200 U/μl Superscript III reverse transcriptase. The mixture was mixed briefly, centrifuged and incubated for 1 h at 50 °C, followed by inactivation at 85 °C for 5 min. The standard curve was generated using purified *MDR1* siRNA treated in the same manner as above for the minicell-extracted siRNA samples, before performing the reverse transcription reaction. Q-PCR reactions were carried out using the Lightcycler TaqMan Master kit (Roche) following the manufacturer's specifications. A 20× primer/probe solution was made, consisting of forward and reverse primers at 18 μM each and 5 μM TaqMan probe. A master mix including 20× primer/probe mix, 5× TaqMan Master Mix and water to 18 μl was assembled and 18 μl aliquoted per capillary tube. Two μl of cDNA from each standard above or cDNA from the extracted *MDR1* siRNA-loaded, or empty minicells, was used per PCR reaction. Cycling conditions were a 95 °C step for 1 min (one cycle); 95 °C 15 s, 55 °C 1 min (45 cycles) and 4 °C cooling step. Reactions were analyzed using the Lightcycler v 2.0 (Roche).

Mouse and human cytokine and interferon response analyses. Mouse serum was analyzed for human and mouse IFNα, IFNβ, IFNγ, TNF∝ and IL-6, following validation of each ELISA according to the manufacturer's instructions. The IFNα and IFNβ ELISA kits were supplied by PBL Biomedical laboratories and the IFNγ, TNF∝ and IL-6 ELISA duoset kits were supplied by R&D Systems. Each ELISA was developed using the 3,3′,5,5′′-tetramethylbenzidine (Sigma) substrate. Mouse serum samples were diluted 1 in 5 in assay buffer and the standard curves were prepared in 20% FBS for the R&D kits. Microwell plates were read in a Biotek uQuant plate reader at 450 nm with 540 nm as the reference wavelength. KC junior software was used to fit 4 parameter logistic curves to the standards and interpolate the samples. The minimum detectable concentration (MDC) of each assay was calculated by multiplying the s.d. of the response by 10 and dividing by the slope of the standard curve at the inflection point[42].

Dissociation rate constant of anti-O-polysaccharide monoclonal antibody. BIAcore 2000 instrument (GE Healthcare, USA; Macquarie University) was used to determine the dissociation rate constant (K_d) of the anti-Opolysaccharide component of the bispecific antibody. The affinity constant of anti-EGFR monoclonal antibody (mAb 528) has been reported in several previous studies[44–46] and shown to be $\sim 2.5 \times 10^{-9}$ M. The experiment was carried out by taking anti-*S. typhimurium* LPS monoclonal antibody (Biodesign International), diluting it in 10 mM sodium acetate (pH 5.0) and then immobilizing it on a CM5 sensor chip using the amine coupling reaction as

described by the manufacturer. The surface of the chip consisting of flow cell (FC)-1, 2, 3 and 4 was activated by exposing it to a mixture of 200 mM *N*-ethyl-*N*_-dimethylaminopropyl carbodiimide (EDC) and 50 mM *N*-hydroxy-succinimide (NHS) for 7 min. FC-1 was used as a reference surface and was directly deactivated by injecting 1 M ethanolamine at pH 8.5 for 7 min. The other flow cell was injected with anti-LPS antibody, and then with 1 M ethanolamine to block the unreacted groups on the surface. The baseline was allowed to stabilize for at least 1 h in PBS running buffer before injecting test samples. Minicells at a concentration of 2×10^{10}/ml in PBS were injected and ligand association was carried out for 3 min followed by the injection of PBS to permit dissociation to occur over 1 min. Binding assays were performed at 25 °C in PBS buffer at a flow rate of 10 µl/min. Regeneration of the ligands after each binding study was performed using a 1 min pulse of 10 mM Glycine-HCl, pH 2.5 and then washing with PBS. The real-time reference curve obtained from a non-ligand coated flow cell exposed to the PBS buffer was subtracted from binding curves obtained from the flowcells with immobilized ligands. Dissociation rate constants were calculated by nonlinear curve fitting of the primary sensogram data using Bioevaluation 3.1 software.

32. Weil, D. *et al.* Targeting the kinesin Eg5 to monitor siRNA transfection in mammalian cells. *Biotechniques* **33**, 1244–1248 (2002).
33. Wu, H., Hait, W.N. & Yang, J.M. Small interfering RNA-induced suppression of MDR1 (P-glycoprotein) restores sensitivity to multidrug-resistant cancer cells. *Cancer Res.* **63**, 1515–1519 (2003).
34. Zheng, J.H., Chen, C.T., Au, J.L. & Wientjes, M.G. Time- and concentration-dependent penetration of doxorubicin in prostrate tumours. *AAPS PharmSci* **3**, 69–77 (2001).
35. Cummings, J. Method for determination of 4′-deoxydoxorubicin, 4′-deoxydoxorubicinol and their 7-deoxyaglycones in human serum by HPLC. *J. Chromatog.* **341**, 401–409 (1985).
36. Itoh, T. *et al.* Biliary excretion of irinotecan and its metabolites. *J. Pharm. Pharm. Sci.* **7**, 13–18 (2004).
37. Sharma, A. *et al.* Activity of paclitaxel liposome formulations against human ovarian tumor xenografts. *Int. J. Cancer* **71**, 103–107 (1997).
38. Larson, R.R., Khazaeli, M.B. & Dillion, H.K. Development of an HPLC method for simultaneous analysis of five antineoplastic agents. *Appl. Occup. Environ. Hyg.* **18**, 109–119 (2003).
39. Sun, J. *et al.* Antitumor efficacy of a novel class of non-thiol-containing peptidomimetic inhibitors of farnesyltransferase and geranylgeranyltransferase I: combination therapy with the cytotoxic agents cisplatin, taxol and gemcitabine. *Cancer Res* **59**, 4919–4926 (1999).
40. Sambrook, J. *et al. Molecular Cloning: Laboratory Manual 3rd ed.* (Cold Spring Harbor Laboratory Press, Cold Spring Harbor, New York, 2001).
41. Ausubel, F.M. *et al. Current Protocols in Molecular Biology.* (John Wiley & Sons, Inc, Hoboken, New Jersey, 2003).
42. Chen, C. *et al.* Real-time quantification of microRNAs by stem-loop RT-PCR. *Nucleic Acids Res.* **33**, e179 (2005).
43. Raymond, C.K., Roberts, B.S., Garrett-Engele, P., Lim, L.P. & Johnson, J.M. Simple, quantitative primer-extension PCR assay for direct monitoring of microRNAs and short interfering RNAs. *RNA* **11**, 1737–1744 (2005).
44. Kawamoto, T. *et al.* Growth stimulation of A431 cells by epidermal growth factor: identification of high-affinity receptors for epidermal growth factor by an anti-receptor monoclonal antibody. *Proc. Natl. Acad. Sci. USA* **80**, 1337–1341 (1983).
45. Sato, J.D. *et al.* Biological effects in vitro of monoclonal antibodies to human epidermal growth factor receptors. *Mol. Biol. Med.* **1**, 511–529 (1983).
46. Reilly, R.M. *et al.* A comparison of EGF and MAb 528 labeled with 111In for imaging human breast cancer. *J. Nucl. Med.* **41**, 903–911 (2000).

doi:10.1038/nbt.1547